Journal of Alzheimer's Disease 23 (2011) 37–48
DOI 10.3233/JAD-2010-100270
IOS Press



# *In vivo* Detection of Amyloid Plaques in the Mouse Brain using the Near-Infrared Fluorescence Probe THK-265

Nobuyuki Okamura[a,b,*], Masanori Mori[a,b], Shozo Furumoto[a,c], Takeo Yoshikawa[a], Ryuichi Harada[a], Satoshi Ito[a], Yosuke Fujikawa[a], Hiroyuki Arai[d], Kazuhiko Yanai[a] and Yukitsuka Kudo[b]
[a]*Department of Pharmacology, Tohoku University School of Medicine, Sendai, Japan*
[b]*Innovation of New Biomedical Engineering Center, Tohoku University, Sendai, Japan*
[c]*Division of Radiopharmaceutical Chemistry, Cyclotron and Radioisotope Center, Tohoku University, Sendai, Japan*
[d]*Institute of Development, Aging and Cancer, Tohoku University, Sendai, Japan*

Handling Associate Editor: Victor Villemagne

Accepted 3 September 2010

**Abstract.** Noninvasive detection of amyloid-β (Aβ) deposits in the brain would be beneficial for an early and presymptomatic diagnosis of Alzheimer's disease (AD). We developed THK-265 as a candidate near-infrared fluorescence (NIRF) probe for the *in vivo* detection of amyloid deposits in the brain. The maximal emission wavelength of THK-265 was greater than 650 nm and it showed high quantum yield and molar absorption coefficients. A fluorescence binding assay showed its high binding affinity to Aβ fibrils (Kd = 97 nM). THK-265 clearly stained amyloid plaques in AD neocortical brain sections and showed a moderate log *p* value (1.8). After intravenous administration of THK-265 in amyloid-β protein precursor (AβPP) transgenic mice, amyloid deposits in the brain were clearly labeled with THK-265. Furthermore, *in vivo* NIRF imaging demonstrated significantly higher fluorescence intensity in the brains of AβPP transgenic mice than in those of wild-type mice. As THK-265 showed profound hyperchromic effect upon binding to Aβ fibrils, good discrimination between AβPP transgenic and wild-type mice was demonstrated even early after THK-265 administration. Furthermore, the fluorescence intensity of THK-265 correlated with amyloid plaque burden in the brains of AβPP transgenic mice. These findings strongly support the usefulness of THK-265 as an NIRF imaging probe for the noninvasive measurement of brain amyloid load.

Keywords: Alzheimer's disease, amyloid, amyloid-β protein, fluorescence, molecular imaging

## INTRODUCTION

The pathological hallmark of Alzheimer's disease (AD) is the deposition of senile plaques and neurofibrillary tangles, as well as the destruction of neurons [1]. Senile plaques are composed of amyloid-β (Aβ) protein. Aβ is a 4-kDa, 39–43 amino acid product derived from the proteolytic cleavage of amyloid-β protein precursor (AβPP) by β- and γ-secretases. Abnormal accumulation of senile plaques has been implicated as a critical event in the etiology and pathogenesis of AD [2] and it precedes cognitive deterioration [3]. Thus, the *in vivo* detection of senile plaques in the brain enables us to identify patients with AD in the presymptomatic stage of the disease [4, 5]. Many β-sheet binding agents have been

*Correspondence to: Nobuyuki Okamura, MD, PhD, Department of Pharmacology, Tohoku University School of Medicine, 2–1 Seiryo-machi, Aoba-ku, Sendai 980–8575, Japan. Tel.: +81 22 717 8058; Fax: +81 22 717 8060; E-mail: oka@mail.tains.tohoku.ac.jp.

ISSN 1387-2877/11/$27.50 

developed as radiotracers for positron emission tomography (PET) and single photon emission computed tomography (SPECT) [6, 7]. Clinical PET studies using [$^{11}$C]6OH-BTA-1 (PiB), [$^{18}$F]FDDNP, [$^{11}$C]SB-13, [$^{11}$C]BF-227, [$^{11}$C]AZD2184, [$^{18}$F]BAY94-9172, [$^{18}$F]GE067, and [$^{18}$F]AV45 have shown a robust difference between the retention pattern of AD patients and healthy controls; AD patients showed a significantly higher tracer retention in the neocortical areas of the brain that are affected by Aβ deposition [8–15]. Molecular imaging with PET has some advantages such as high sensitivity and quantitative ability over other noninvasive imaging techniques. However, PET imaging generally requires a local cyclotron for generating short-lived positron-emitting radionuclides and a synthetic unit to produce radiolabeled agents. Thus, increasing interest has been focused on finding other relatively inexpensive methods that can be applied to widespread screening for brain amyloid deposition.

As an alternative to PET, near-infrared fluorescence (NIRF) imaging is expected to have a major impact on molecular Aβ imaging [16, 17]. In general, biological tissues exhibit high photon absorbance both in the visible wavelength range (350–600 nm) and in the infrared range (>900 nm). However, the absorbance decreases to a minimum in the near-infrared region (600–900 nm), also referred to as the "optical window". Therefore, a non-invasive imaging technique using NIRF probes offers a unique advantage for *in vivo* molecular imaging [18–20]. A previous study using the NIRF dye AOI987 successfully demonstrated the *in vivo* detection of amyloid plaques in the mouse brain [18]. We screened NIRF compounds for use as *in vivo* amyloid imaging agents and discovered 5-(2E,4E)-5-(6-hydroxy-4-oxo-2-thioxo-1,2,3,4-tetrahydroxy-5-pyrimidinyl)-2,4-pentadienylidene-2-thioxodihydro-4,6(1H,5H)-pyrimidinedione (THK-265) as a candidate NIRF imaging probe. In this study, we report the optical and binding profiles of THK-265 and demonstrate *in vivo* NIRF imaging of amyloid deposits using this probe in an animal model of AD.

## MATERIALS AND METHODS

### *Measurement of excitation and emission spectra*

THK-265 (molecular weight 350.38; Fig. 1) was purchased from Organica (Wolfen, Germany) and custom purified by Tanabe R&D Service (Osaka, Japan). To analyze the THK-265 fluorescence spectra, the compound was dissolved in 100% methanol, 50 mM potassium phosphate buffer (pH 7.4), or human serum (Gemini Bio-Products, West Sacramento, CA, USA). To measure the excitation and emission spectra of the THK-265/Aβ fibril complex, 20 μM of $A\beta_{1-40}$ (Peptide Institute, Osaka, Japan) in 50 mM of potassium phosphate buffer was incubated at 37°C on a Vibrax VXR shaker (IKA, Cincinnati, OH, USA) for 4 days. Before the fluorometric measurements, the Aβ solution was sonicated for 15 min at 45 kHz using a VS-100III ultrasonic cleaner (Iuchi, Osaka, Japan). Excitation and emission spectra were recorded using a FP-6300-WRE-362 spectrofluorometer (Jasco, Tokyo, Japan) at a scan rate of 100 nm/min. THK-265 excitation and emission spectra were recorded at a concentration of 1 μM in a quartz cuvette with and without 5 μM of aggregated $A\beta_{1-40}$ in 50 mM of potassium phosphate buffer.

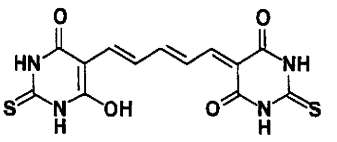


Fig. 1. Chemical structure of THK-265.

### *Measurement of absorption coefficient and quantum yield*

THK-265 (1 μM final concentration) was dissolved in 100% methanol or 50 mM potassium phosphate buffer (pH 7.4) to measure quantum yield. $A\beta_{1-40}$ (20 μM) in 50 mM potassium phosphate buffer was incubated at 37°C on a Vibrax VXR shaker at 500 rpm for 4 days. Before the fluorometric measurement, the Aβ solution was sonicated for 15 min at 45 kHz using an ultrasonic cleaner. The number of emitted photons and photons absorbed by the sample were measured in 5 μM of THK-265, with and without 5 μM of aggregated $A\beta_{1-40}$ in 100% methanol or 50 mM of potassium phosphate buffer using an absolute photoluminescence (PL) quantum yield measurement system (C9920–02, Hamamatsu Photonics, Hamamatsu, Japan) for THK-265. PL quantum yields are given as the ratio of the number of photons emitted to the number of photons absorbed. The molar absorption coefficient was obtained from the equation $\varepsilon = A/(c \times l)$, where $A$ is the actual absorbance of light, $c$ is the molar concentration of the THK-265 solution, and $l$ is the path length (cm). The light absorbance of the THK-265 solution was measured using a UV-2550 spectrophotometer (Shimadzu, Kyoto, Japan).

*Measurement of octanol/water partition coefficient*

To measure the octanol/water partition coefficient of THK-265, saturated potassium phosphate buffer and 1-octanol (Wako, Osaka, Japan) were prepared before measurement as described previously [11]. THK-265 was dissolved in saturated potassium phosphate buffer and shaken with equal amounts of saturated 1-octanol for 30 min at room temperature. After centrifugation at 2000 rpm for 15 min, the fluorescence intensity of THK-265 in the potassium phosphate buffer layer was measured at an excitation wavelength of 630 nm and an emission wavelength of 670 nm using a GEMINI XS microplate spectrofluorometer (Molecular Devices, Sunnyvale, CA, USA). Octanol/water partition coefficients were determined by comparing fluorescence intensity with that measured before shaking with 1-octanol. Measurements were performed in triplicate.

*Measurement of THK-265 brain uptake in mice*

Brain uptake of intravenously administered THK-265 in mice was measured using an HPLC system with a fluorescence detector. THK-265 (1 mg/kg), dissolved in saline, ethanol, and NaOH, were administered into the tail vein of male ICR mice (7-week-old, 32 g, $n = 3$). At 2 and 30 min after the injection of compounds, blood samples were collected from the heart, and then the brain was dissected out under ether anesthesia. Blood samples were centrifuged at 10000*g* for 5 min to obtain the plasma. Brain samples were homogenized in 2 ml of saline. Brain homogenates were centrifuged at 4,000 rpm for 10 min, and the supernatant was diluted ten-fold with 20 mM $NaH_2PO_4$. A Speedisk column (J.T. Baker, Phillipsburg, NJ, USA) was conditioned with 2 ml of acetonitrile, 2 ml of methanol, and 2 ml of distilled water before use. The sample was passed through the column followed by air dehydration and then eluted with 0.5 ml of methanol. For standards, 0.5, 5, 50, and 500 ng/ml of THK-265 were mixed with plasma or brain homogenate. Samples were analyzed using an HPLC system (Nanospace SI-2, Shiseido, Tokyo, Japan). The mobile phase was 20 mM $NaH_2PO_4$ (pH 6.5) and acetonitrile at a flow rate of 1 ml/min. The fluorescence detector was operated at an excitation and emission wavelength of 627 and 649 nm, respectively. The plasma and brain THK-265 concentrations were calculated using peak areas for the samples and standard. The concentration reported is an average ± standard deviation of three independent experiments. THK-265 brain uptake in mice was additionally measured by *ex vivo* fluorescence imaging of brain samples. THK-265 (1 mg/kg) dissolved in saline, ethanol, and NaOH were injected into the tail vein of male ICR mice (7-week-old, 32 g, $n = 12$). The mice were perfused intracardially with saline under ether anesthesia, and then sacrificed before ($n = 3$) and 2 min ($n = 4$), 60 min ($n = 4$), and 120 min ($n = 4$) after the injection of THK-265. The brain was dissected out, and the fluorescence intensities of brain samples were examined using an IVIS100 imaging system (Xenogen, Alameda, CA, USA). A Cy5.5 filter set (excitation 615–665 nm, emission 695–770 nm) was used for acquiring THK-265 fluorescence, because the excitation wavelength of this filter set was optimal among the available filters.

*In vitro fluorescence binding assay*

A fluorometric analysis of THK-265 binding with Aβ fibrils was performed using the following method. $A\beta_{1-40}$ or $A\beta_{1-42}$ (20 μM; Peptide Institute) in 50 mM potassium phosphate buffer (pH 7.4) was incubated at 37°C on a Vibrax VXR shaker for 4 days. Before the fluorometric analysis, the Aβ fibril solutions were sonicated for 3 min at 45 kHz using a VS-100III ultrasonic cleaner. Fluorescence spectra for the mixture of 5 μM Aβ fibrils and different concentrations of THK-265 (3, 10, 30, 100, 300 nM, and 1 μM final concentrations) were measured using a GEMINI XS microplate spectrofluorometer at an excitation wavelength of 650 nm and an emission wavelength of 670–770 nm. Fluorescence spectra for the same THK-265 concentrations were also measured without the Aβ fibril mixture or with a soluble Aβ mixture. Spectra of the difference in fluorescence intensity (ΔF) between solutions with and without the $A\beta_{1-40}$ fibril mixture were calculated for each THK-265 concentration. The maximum ΔF was used as an index of THK-265-specific binding to fibrillar Aβ. The binding constant (Kd) of THK-265 to Aβ was calculated from a plot of THK-265 concentration versus ΔF of THK-265 at an emission wavelength of 680 nm using GraphPad Prism software (GraphPad, San Diego, CA, USA).

*Tissue staining*

Postmortem brain tissues from an autopsy-confirmed AD case (69-year-old man) were obtained from Fukushimura Hospital (Toyohashi, Japan). Serial sections (8 μm thickness) from paraffin-embedded blocks of the temporal cortex were prepared in xylene and ethanol. Tissue sections were immersed in 100 μM

of THK-265 solution for 10 min. Stained sections were then dipped briefly into water, rinsed in phosphate-buffered saline (PBS), and examined using a fluorescence microscope (Eclipse 80i; Nikon, Tokyo, Japan) equipped with a Cy5.5 filter set (excitation 615–665 nm, emission 695–770 nm). In addition, the adjacent section was immunostained using a monoclonal antibody (mAb) against Aβ (6F/3D; Dako, Glostrup, Denmark) and tau (AT8; Innogenetics, Ghent, Belgium). Sections were immersed in a solution containing 6F/3D at a dilution rate of 1 : 50 for 60 min or AT8 at a dilution of 1 : 20 for 18 h. Sections were processed by the avidin-biotin method using a Pathostain ABC-POD(M) kit (Wako, Osaka, Japan).

*Ex vivo labeling of Aβ deposits with THK-265 in transgenic mice*

Animal experiments in this report were approved by the ethical committee for animal experiments of Tohoku University. *Ex vivo* plaque labeling with THK-265 was examined using 3 transgenic (Tg) AβPPSwe Tg2576 mice (Taconic, Germantown, NY, USA) and 2 wild-type (Wt) mice (female, 17-month-old). In addition, indocyanine green (ICG; Diagnogreen, Daiichi Sankyo, Tokyo, Japan) was used as negative control. ICG or THK-265 solution containing 0.1 M PBS, 10% dimethyl sulfoxide, and 0.02 mol/l HCl was injected into the tail vein at a dose of 1 mg/kg. At 5 min after the injection, the mice were perfused intracardially with saline under ether anesthesia. Mice were then decapitated, and their brains were removed. After cryoprotection in 30% sucrose/0.1 M PBS, 16-μm frozen sections were cut using a Microm HM560 cryostat (Walldorf, Germany) and imaged for fluorescent microscopy with no additional staining using a Cy5.5 filter set. The same sections were immersed in 0.125% thioflavin-S solution containing 50% ethanol for 3 min, dipped five times briefly in tap water, followed by differentiation in 50% ethanol for 2 min. The sections were then examined using a Nikon Eclipse 80i microscope equipped with a BV-2A filter set (excitation 400–440 nm, emission 470 nm cut on).

*In vivo NIRF imaging of Aβ deposits with THK-265 in transgenic mice*

Female AβPPSwe Tg2576 mice aged 17 months ($n=3$), 19 months ($n=3$), 27 months ($n=3$), and 32 months ($n=3$) as well as age-matched Wt mice were used to assess the potential of THK-265 as an amyloid imaging agent. AOI987 and ICG were used as positive and negative controls, respectively. AOI987 was custom synthesized by Tanabe R&D Service Co. (Osaka, Japan). *In vivo* fluorescence signals were measured using an IVIS100 imaging system (Xenogen). This instrument is a temperature-controlled, light-tight box with a cryogenically cooled, back-illuminated, digital charge-coupled device camera. Fluorescent signals were measured and analyzed with Living Image software (Xenogen). The fluorescence reflectance imaging technique is sensitive to the coat color. Thus, the same coat-colored (brown) mice were used for this experiment. Before the experiment, the heads and necks were shaved to minimize the inherent autofluorescence from hair. Mice were anesthetized with isoflurane (Dainippon Pharmaceutical Co., Osaka, Japan) before they were placed in IVIS100. It is possible that inconsistent placement of the mice could lead to variations within the field of view. Therefore, the mice were fixed in the stereotaxic instrument during the experiment. Mice were then injected with 1 mg/kg of THK-265, AOI987, or ICG via the tail vein. Images were acquired for 120 min under isoflurane anesthesia. A Cy5.5 filter set was used for acquiring THK-265 and AOI987 fluorescence, and an ICG filter set (excitation 710–760 nm, emission 810–875 nm) was used for acquiring ICG fluorescence *in vivo*. Identical illumination settings were used for all images, and fluorescence emission was normalized to photons per second per centimeter square per steradian (p/s/cm$^2$/sr). For the comparative analysis of three compounds, the circular regions of interest (ROI) (7.5 mm in diameter) were set on the heads (ROI1) and necks (ROI2) of each mouse (Fig. 2). The head-to-neck fluorescence intensity ratio (ROI1/ROI2) of each compound was calculated and used as an index of the compound's retention in the brain, because the neck is a region free of amyloid deposits in AβPP Tg mice. After finishing the *in vivo* measurement of THK-265 fluorescence signals, mice were decapitated and their brains were removed. After cryoprotection, 16-μm frozen sections were cut using a HM560 cryostat. To examine the correlation between THK-265 fluorescence intensity and amyloid burden in AβPP Tg mice, the number of amyloid plaques stained with 0.125% thioflavin-S was determined in 4 sections (spaced 480 μm apart) from whole brain in each mouse.

*Toxicity study in mice*

An acute toxicity study was performed using female ICR mice (weight, 29–34 g). Animals were kept in a temperature-controlled environment (21.2–23.5°C)

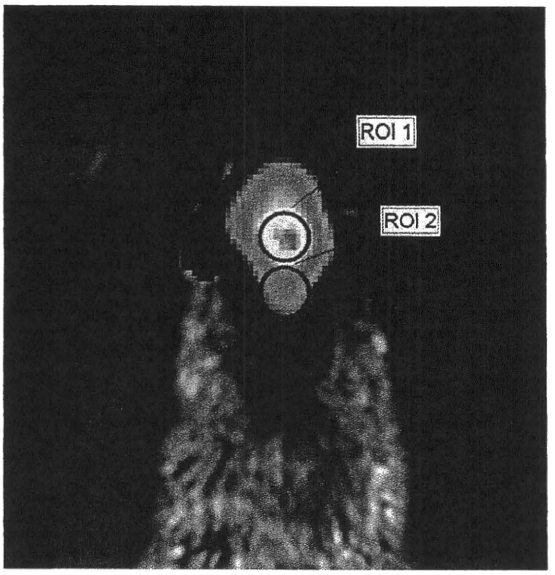


Fig. 2. Placement of regions of interest (ROIs) on the mouse head (ROI1) and neck (ROI2).

with a 12-h light-dark cycle and *ad libitum* access to food and water. Animals were divided into control and treated groups, with four animals in each group. The control group received a vehicle injection alone, while the treated group received an intravenous injection of THK-265 solution at a dose of 10 mg/kg. Animals were observed for 7 days after administration to identify any changes in general behavior or body weight.

*Statistical analysis*

Statistical comparison of fluorescence measurements was performed by analysis of variance followed by a Bonferroni multiple comparisons test with a significance level of $p < 0.05$. Correlations between the number of amyloid plaques and fluorescence intensity ratio were examined using a non-parametric Spearman's rank correlation analysis. These analyses were performed using GraphPad Prism software.

## RESULTS

*Fluorescence properties of THK-265*

The maximum excitation and emission wavelengths of the THK-265 solution were 639.0 nm and 657.4 nm in human serum, 620.0 nm and 648.0 nm in potassium phosphate buffer, and 627.0 nm and 644.0 nm in methanol, respectively. In addition, the maximum excitation and emission wavelengths of the THK-265/Aβ

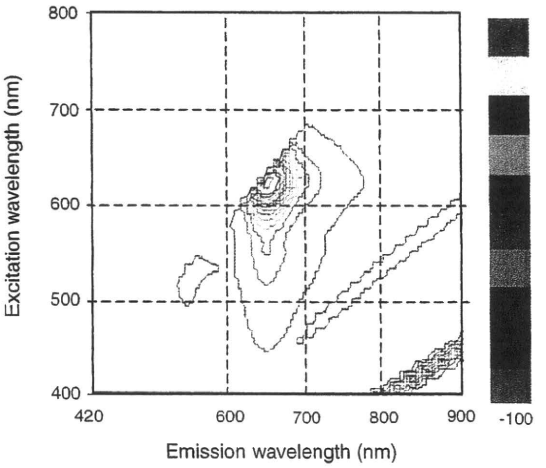


Fig. 3. Fluorescence contour map of the THK-265/amyloid-β fibril complex.

fibril complex were 630.0 nm and 650.0 nm, respectively (Fig. 3). These values were within the optical window range, suggesting that the fluorescence signal of this compound is capable of passing through body tissue. Furthermore, this compound showed a high quantum yield (38.5% in methanol solution) and high molar absorption coefficients (96198 $M^{-1}cm^{-1}$ in methanol solution).

*Binding of THK-265 to Aβ fibrils and AD pathology*

The fluorescence intensity of THK-265 increased 3.6 times after it was mixed with $A\beta_{1\text{-}40}$ fibrils ($196.9 \pm 2.8$ p/s) and 6 times higher after it was mixed with $A\beta_{1\text{-}42}$ fibrils ($325.9 \pm 5.7$ p/s) compared to that without mixing with Aβ fibrils ($54.4 \pm 1.9$ p/s) (Fig. 4A). However, no increase in THK-265 fluorescence was observed in the mixture with soluble Aβ peptide. These findings reflect the hyperchromic fluorescence shift of THK-265 upon binding to Aβ fibril β-sheet structures. The ΔF spectra in the different THK-265 concentrations are shown in Fig. 4B. The ΔF value increased with increasing THK-265 concentration, and the calculated Kd value of THK-265 to Aβ was $97 \pm 5.0$ nM (Fig. 4C). A neuropathological examination using THK-265 indicated that amyloid plaques were clearly stained with THK-265 in AD brain sections (Fig. 5A). This staining pattern correlated well with Aβ immunostaining in adjacent sections (Fig. 5B). Cored plaques were clearly stained with THK-265 (Fig. 5A); however, diffuse plaques were not clearly stained with THK-265 (data not shown).

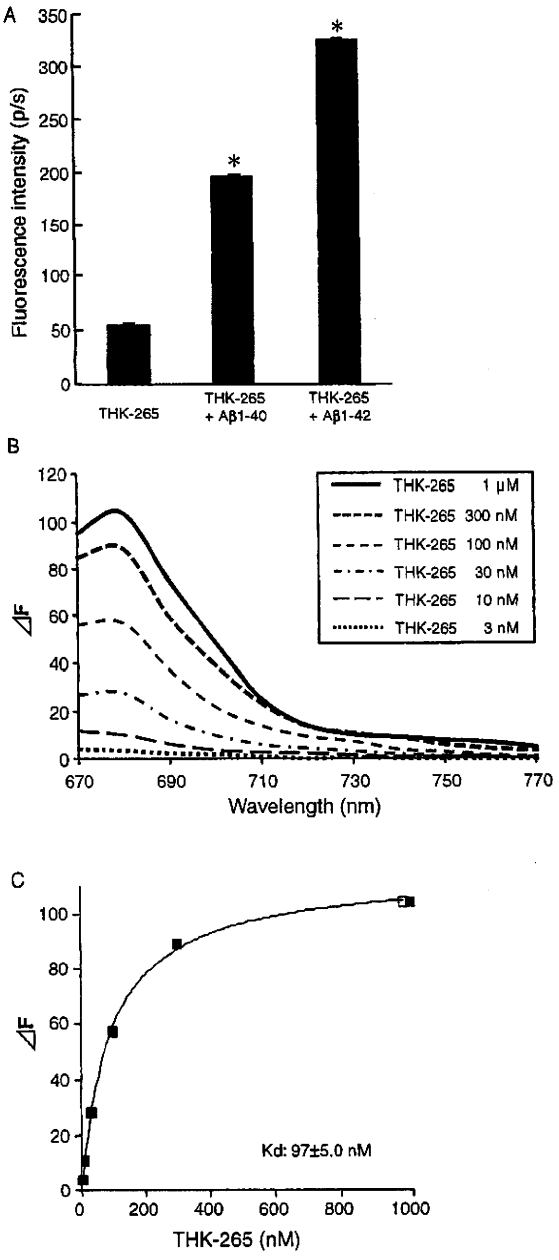


Fig. 4. *In vitro* binding of THK-265 to amyloid-β (Aβ) fibrils. A) Comparison of THK-265 fluorescence intensity and that of the THK-265/Aβ fibril complex. B) Difference in the fluorescence emission spectra of the THK-265/Aβ fibril complex. C) Saturation curve of THK-265 binding to Aβ fibrils. $*p < 0.05$, compared with fluorescence intensity of THK-265 only.

Neurofibrillary tangles were additionally stained with THK-265 (Fig. 5C, D). Amyloid plaques stained with THK-265 were located in the surface region of the AD frontal cortex (Fig. 5E, F).

*Brain uptake of THK-265 in mice*

We measured the octanol/water partition coefficient of THK-265 to investigate whether THK-265 would enter the brain in amounts sufficient for *in vivo* detection of amyloid plaques. The octanol/water partition coefficient and its log $p$ value were $66 \pm 6.2$ and $1.8 \pm 0.8$, respectively, indicating that THK-265 was sufficiently lipophilic to permeate the blood brain barrier (BBB). Brain uptake of THK-265 in mice was measured by an HPLC system with a fluorescence detector. THK-265 displayed brain uptakes of $0.04 \pm 0.01\%$ injected dose (ID)/g at 2 min post injection (PI) and $0.0065 \pm 0.0026\%$ID/g at 30 min PI. Brain uptake of THK-265 was additionally measured by *ex vivo* fluorescence imaging of brain samples in mice (Fig. 6). THK-265 rapidly entered the brain ($6.2 \pm 1.9 \times 10^7$ p/s/cm$^2$/sr) at 2 min PI, and then gradually eliminated from the brain ($2.4 \pm 0.6 \times 10^7$ p/s/cm$^2$/sr at 60 min PI and $2.1 \pm 0.8 \times 10^7$ p/s/cm$^2$/sr at 120 min PI).

*Toxicity study of THK-265*

In the acute toxicity study, intravenous administration of THK-265 at a dose of 10 mg/kg did not produce any significant changes in the general behavior or body weight of mice. During the 7 days of the experiment, no deaths occurred in either the control or treatment groups, indicating that the dose for 50% lethality ($LD_{50}$) of intravenously administered THK-265 is higher than 10 mg/kg in mice.

*Ex vivo labeling of Aβ deposits in transgenic mice with THK-265*

Next, *in vivo* binding ability to intracranial THK-265 amyloid deposits was confirmed by intravenous administration of 1 mg/kg THK-265 to 17-month-old AβPP Tg and Wt mice. As a result, amyloid deposits in 3 Tg mice were clearly labeled with THK-265 (Fig. 7A, C, E). In contrast, no significant THK-265 fluorescence was observed in the brain of Wt mice (data not shown). The distribution of plaques labeled with THK-265 corresponded to thioflavin-S staining (Fig. 7B, D, F), indicating that intravenously administered THK-265 enters the brain and selectively binds to intracranial amyloid deposits. In contrast, ICG did not label amyloid deposits in Tg mouse brain after intravenous administration (Fig. 7G, H).

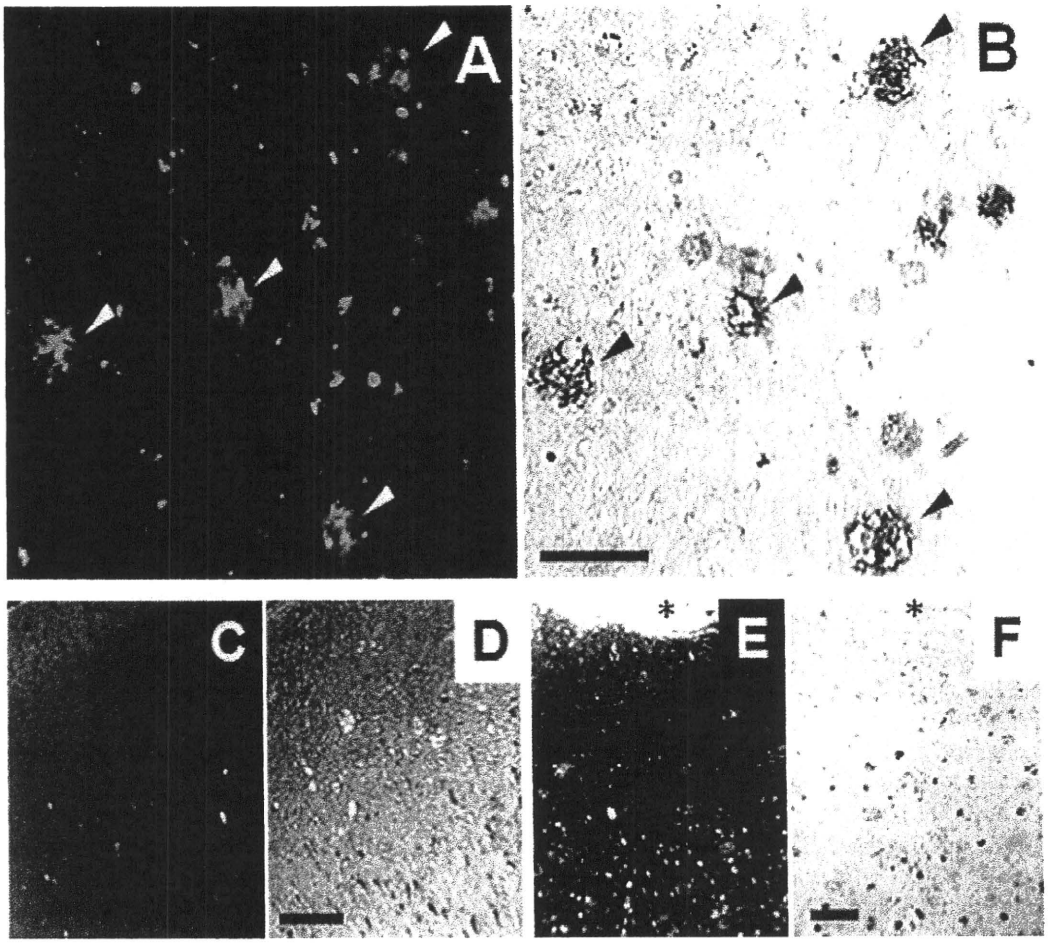


Fig. 5. Microscopic images of THK-265 binding to amyloid plaques and neurofibrillary tangles. A) THK-265 staining of the temporal cortex from a patient with Alzheimer's disease (AD). B) Aβ immunostaining in the adjacent section of the AD temporal cortex. Arrowheads indicate amyloid plaques. C) THK-265 staining of the hippocampus of an AD patient. D) Tau immunostaining in the adjacent section of the AD hippocampus. E) THK-265 staining and (F) Aβ immunostaining of the frontal cortex from an AD patient. Asterisks indicate brain surface. Bar = 100 μm.

*In vivo NIRF imaging of Aβ deposits in transgenic mice by THK-265*

Finally, we examined the ability of THK-265 to detect amyloid plaques noninvasively using NIRF imaging. After intravenously injecting 1 mg/kg THK-265, fluorescence intensity rapidly increased in mice heads and was consistently higher in Tg than in Wt mice (Fig. 8A–C). Moreover, THK-265 fluorescence intensity increased with increasing age in Tg mice, which is consistent with the observation of higher density amyloid deposits in the brains of 32-month-old Tg mice than in that of 19-month-old Tg mice (data not shown). In contrast, Wt mice showed no age-related increase in THK-265 fluorescence intensity in the brain (Fig. 8C). When comparing THK-265 with AOI987 and ICG, both THK-265 and AOI987 displayed significantly higher fluorescence signals in AβPP Tg mice than in Wt mice. However, ICG showed no significant difference in fluorescence signals between AβPP Tg and Wt mice (Fig. 9A, B). When AOI987 was injected into mice, the ratio of fluorescence intensity in AβPP Tg mice to that in Wt mice (AβPP Tg/Wt ratio) increased gradually. In contrast, THK-265 showed a consistently high AβPP Tg/Wt ratio at 30 min PI and significantly higher AβPP Tg/Wt ratio than AOI987 between 30 and 90 min PI (Fig. 9C). As shown in Fig. 9D, the fluorescence THK-265 intensity ratio correlated significantly with the number of amyloid plaques in the brain ($r = 0.943$, $p = 0.017$).

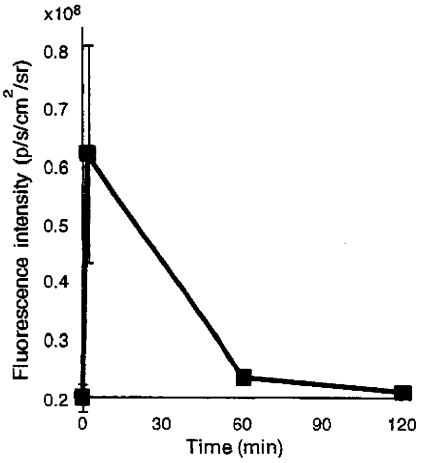


Fig. 6. *Ex vivo* measurement of brain tissue fluorescence intensity after intravenous administration of THK-265 in mice.

## DISCUSSION

Although there has been no evidence supporting good penetration of fluorescence signals through the human head, the NIRF imaging technique is potentially useful for *in vivo* detection of amyloid in the brain. In NIRF imaging, there is no risk from radiation exposure. In addition, it has a lower cost than radionuclide imaging by PET and SPECT [16, 19]. High time resolution of optical imaging additionally allows high-throughput screening for amyloid deposition. Several methodological limitations exist in NIRF imaging. As with radionuclide imaging, quantification of amyloid load is achieved by spatially integrating the fluorescence intensity of the amyloid-binding probe. Because of fluorescence scattering in biological tissue, the spatial resolution and quantitative ability of NIRF imaging is relatively lower than that of radionuclide imaging by PET and SPECT. Large individual differences in fluorescence intensity can be overcome by normalizing the measured fluorescence intensity to that at an initial scan time point or that at a reference region containing no amyloid plaques (e.g., spinal cord), as demonstrated in our study. Radionuclide imaging by PET and SPECT provides full three-dimensional information with high sensitivity. However, the NIRF imaging technique detects the regional density of fluorescence dye mainly on the surface area of the brain; therefore, it is limited to detecting fluorescence dye in deep layers of the brain. However, this weakness does not affect the detectability of amyloid plaques in the human brain, because high density amyloid deposits are located on the neocortical surface of patients with AD, as shown in Fig. 5E, F.

AOI987 is the first successful NIRF probe for *in vivo* detection of Aβ pathology [18]. This probe readily penetrates BBB and binds to amyloid plaques. Using an *in vivo* NIRF imaging device, the specific interaction of AOI987 with amyloid plaques in AβPP23 transgenic mice has been demonstrated. A quantitative analysis revealed increasing fluorescence signal intensity with increasing plaque load of the animals. Significant binding of AOI987 was observed for AβPP23 transgenic mice of age 9 months and older. Thus, AOI987 is an attractive probe to noninvasively monitor disease progression in AβPP Tg mice and to evaluate effects of potential anti-amyloid drugs on the plaque load. There are several requirements for the successful development of an NIRF imaging probe to detect AD-specific pathology [18–20]. One of the most important requirements is a suitable excitation and emission wavelength (600–800 nm) for the fluorescence probe. This property is necessary to minimize the absorption of fluorescence signals into body tissues, particularly hemoglobin and water. The optimal THK-265 excitation and emission wavelengths (excitation wavelength 639.0 nm and emission wavelength 657.4 nm in human serum) are within this range, and are comparable to a previously reported compound, AOI-987. THK-265 additionally showed a high quantum yield (38.5% in MeOH) and a high absorption coefficient (96198 $M^{-1}cm^{-1}$ in MeOH), indicating the ideal fluorescence property of THK-265 as an imaging probe. The $LD_{50}$ of intravenously administered THK-265 is greater than 10 mg/kg for mice. However, further safety analyses are required for future clinical applications of this probe. In addition to these properties, compounds must have high Aβ binding affinity. A fluorescence binding assay showed that the THK-265 Kd value for synthetic Aβ fibrils was $97 \pm 5.0$ nM, indicating a higher binding affinity for Aβ fibrils than for thioflavin-T (Ki = 580 nM) [21] and AOI-987 (Kd = 220 nM) [18]. The THK-265 Kd value indicates a relatively lower affinity compared to the radionuclide imaging ligands PiB (Kd = 4.7 nM) [22] and BF-227 (Ki = 4.3 nM) [11]. However, these parameters are largely dependent on analytical conditions and preparation of Aβ fibrils. THK-265 mainly labeled cored plaques, but not diffuse plaque in AD brain sections. A probe binding selectively to cored plaques would be less subject to Aβ pathology in the normal aging process. Thus, use of this probe will allow detection of the transition from normal aging to the pathological process of AD.

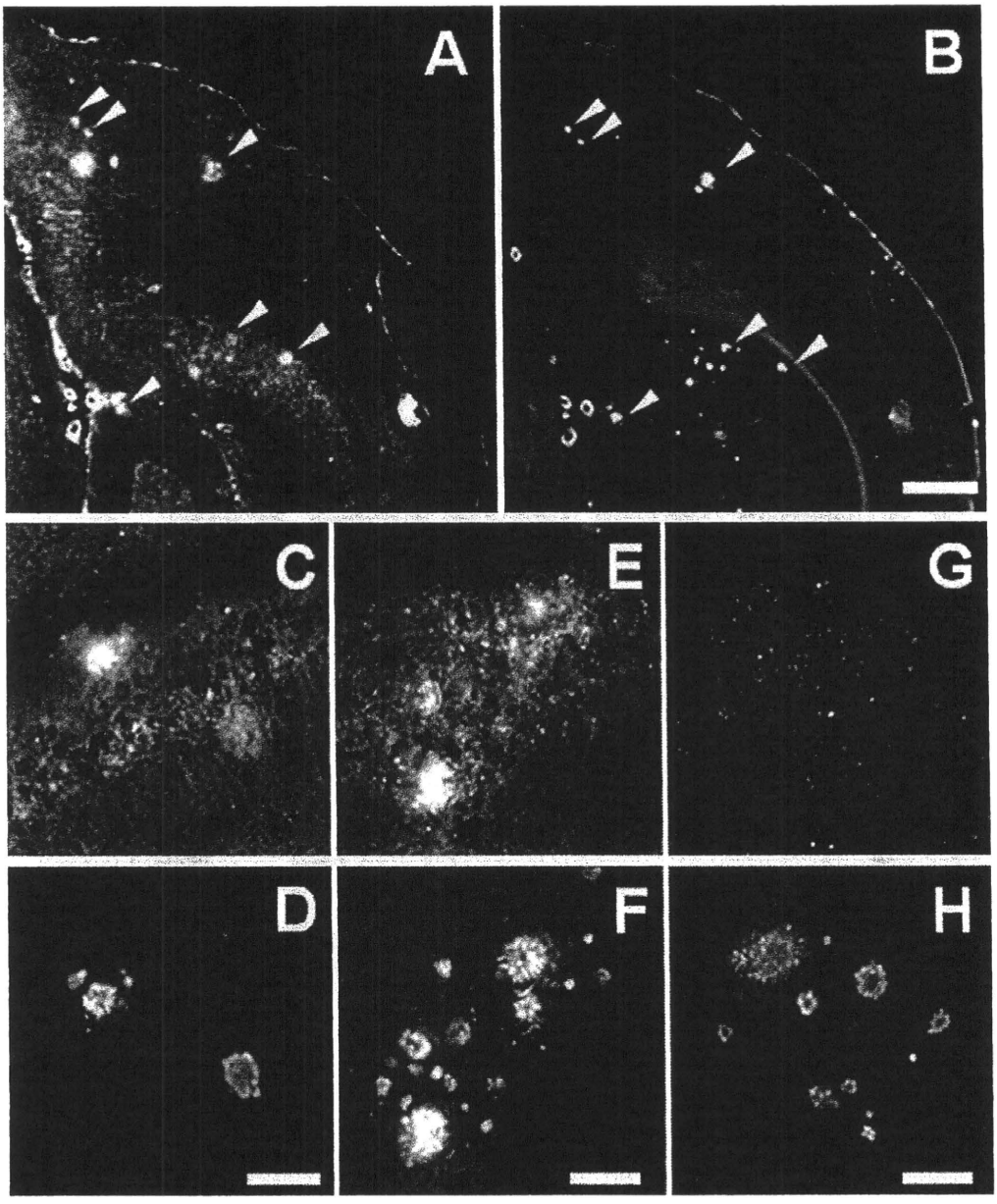


Fig. 7. *Ex vivo* microscopic images of brain sections from 17-month-old amyloid-β protein precursor transgenic mice after intravenous administration of 1 mg/kg THK-265 (A, C, E) or ICG (G). B, D, F, H) Thioflavin-S staining in the same section as (A), (C), (E) and (G), respectively. Arrowheads indicate amyloid plaques. Bar = 500 μm (A, B) and 100 μm (C–H).

One of the advantages of THK-265 over existing amyloid-binding ligands is its profound hyperchromic effect upon binding to Aβ fibrils, which enhances the fluorescence signals derived from the specific binding site, but not the signals from the free compound. Therefore, this effect might compensate for the insufficient binding affinity of THK-265 to Aβ fibrils. During radionuclide imaging, specific tracer binding can be visualized after washing out the remaining background tracer activity. In contrast, the fluorescence dye with a hyperchromic effect enables the enhancement of specific binding. Our study demonstrated good discrimination between specific probe accumulation in transgenic mouse brain and nonspecific probe accumulation in Wt mouse brain, even at the early stage after intravenous THK-265 administration. Actually,

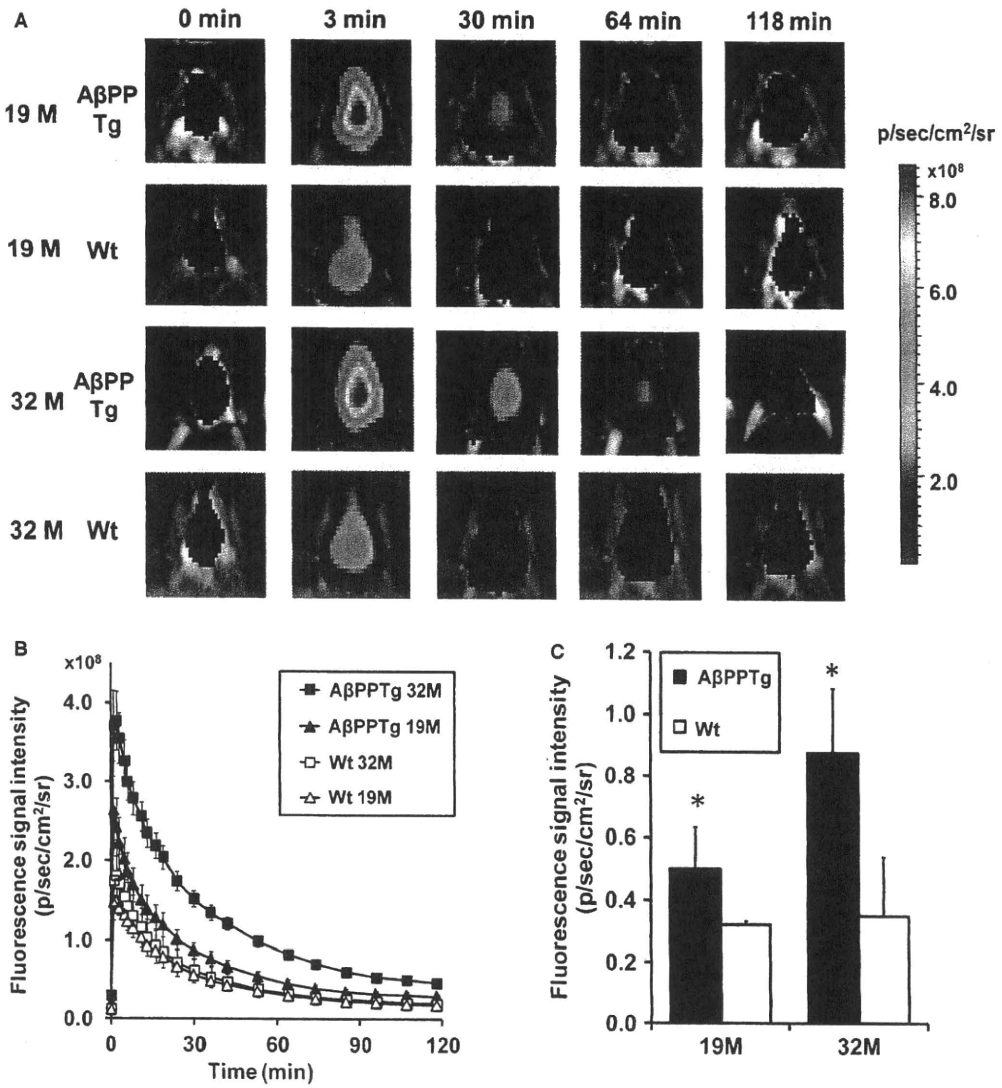


Fig. 8. *In vivo* imaging of amyloid deposits using THK-265. A) Images from the brains of 19-month-old amyloid-β protein precursor (AβPP) transgenic (AβPP Tg) and wild-type (Wt), as well as 32-month-old AβPP Tg and Wt mice acquired before and at 3, 30, 64, and 118 min after intravenous administration of THK-265. B) Fluorescence signal intensities of the heads of 19-month-old and 32-month-old AβPP Tg and Wt mice as a function of time after intravenous administration of THK-265. C) Average fluorescence signal intensities of the heads between 30 and 120 min after THK-265 injection in 19-month-old and 32-month-old AβPP Tg and Wt mice.

*ex vivo* labeling of amyloid plaques was demonstrated at 5 min post-intravenous administration of THK-265 in AβPP Tg mice. These findings are in sharp contrast with previous NIRF probes such as AOI987, which allowed a gradual separation between Wt and Tg mice over a quite long observation period. Thus, a fluorescence probe with a hyperchromic effect would allow an immediate and handy assessment of the plaque burden in living brains. One of the limitations of THK-265 is that it cannot discriminate specific versus non-specific binding of the probe, because no bathochromic shift of THK-265 is observed after binding to Aβ fibrils. The development of a novel probe showing a bathochromic effect or the measurement of lifetime change would solve this problem. In addition, longer excitation and emission wavelengths of the probe would improve the penetration of fluorescence signals in deep brain regions.

BBB permeability is another important requirement for an NIRF imaging probe. Although the brain uptake

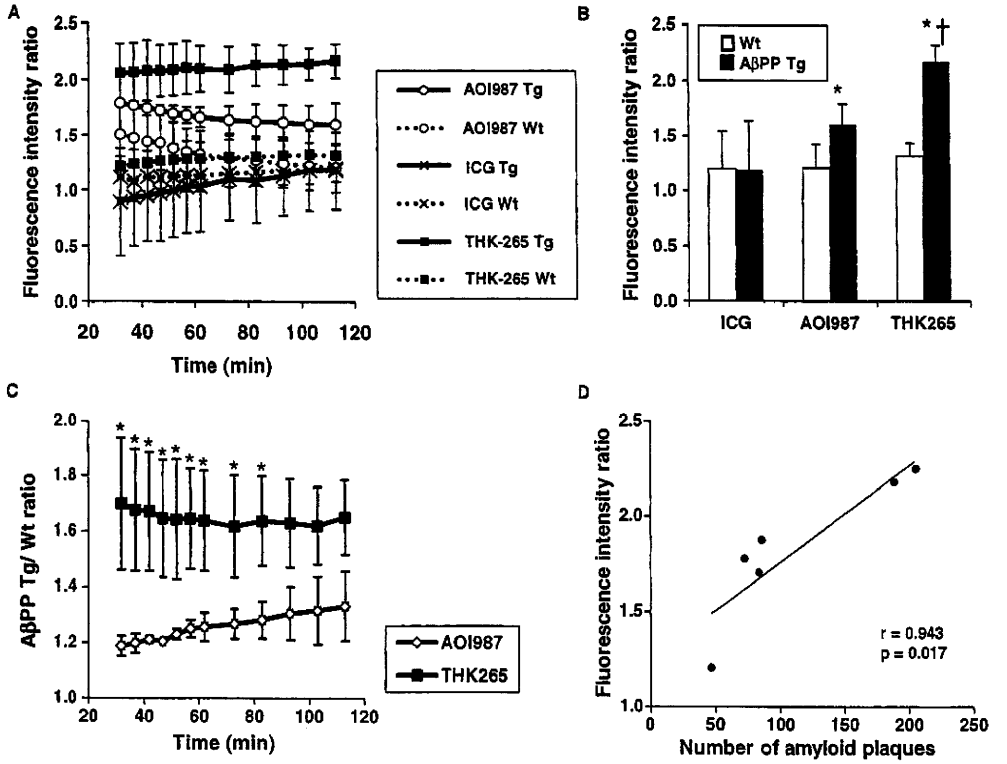


Fig. 9. A) The ratio of head to neck fluorescence intensity of 27-month-old amyloid-β protein precursor transgenic (AβPP Tg) and wild-type (Wt) mice as a function of time after intravenous administration of AOI987 (white circle), ICG (cross) and THK-265 (black square). B) Fluorescence intensity ratio of 27-month-old AβPP Tg and Wt mice at 113 min post injection of THK-265. C) The ratio of fluorescence intensity in 27-month-old AβPP Tg mice to that in Wt mice (AβPP Tg/Wt ratio) as a function of time after intravenous administration of AOI987 (white circle) and THK-265 (black square). D) Significant correlation of the number of amyloid plaques in the brain with fluorescence intensity ratio of THK-265.

level of THK-265 (0.04%ID/g at 2 min post injection) is about 150 times less than most useful PET amyloid probes, our results demonstrated that intravenously administered THK-265 can enter the brain at a level sufficient for *in vivo* detection of amyloid deposits in AβPP Tg mice. After an intravenous injection of THK-265, the mice were perfused, and then brain samples were obtained. Therefore, THK-265 uptake in the brain is not likely to be caused by intravascular dye leaks across BBB following death. These results strongly suggest that NIRF imaging with THK-265 is potentially usable for the noninvasive detection of amyloid plaques in patients with AD. THK-265 showed reasonable lipophilicity ($\log p = 1.8 \pm 0.8$), rapid brain uptake after intravenous administration, and rapid clearing of unbound compound from normal brain tissue in mice. Nevertheless, further compound optimization is needed for future clinical application of this imaging technique.

In summary, we developed a novel NIRF probe, THK-265, for detecting amyloid deposits in the brain *in vivo*. THK-265 showed excellent fluorescence properties as an NIRF agent and high binding affinity to amyloid plaques. Furthermore, we successfully demonstrated that amyloid deposits in AβPP transgenic mice can be detected after intravenous administration of THK-265. From these findings, we concluded that THK-265 is a candidate NIRF probe for the noninvasive detection and monitoring of amyloid deposition.

## ACKNOWLEDGMENTS

This study was supported by the research fund from Sumitomo Electric Industries Ltd, the Small Business Innovation Research (SBIR) program of Japan and the Grant-in-Aid for Scientific Research on Priority Areas "Integrative Brain Research" from the Ministry of Edu-

cation, Culture, Sports, Science, and Technology of Japan (20019006).

Authors' disclosures available online (http://www.j-alz.com/disclosures/view.php?id=607).

## REFERENCES

[1] Vickers JC, Dickson TC, Adlard PA, Saunders HL, King CE, McCormack G (2000) The cause of neuronal degeneration in Alzheimer's disease. *Prog Neurobiol* **60**, 139-165.

[2] Hardy J, Selkoe DJ (2002) The amyloid hypothesis of Alzheimer's disease: progress and problems on the road to therapeutics. *Science* **297**, 353-356.

[3] Price JL, Morris JC (1999) Tangles and plaques in nondemented aging and "preclinical" Alzheimer's disease. *Ann Neurol* **45**, 358-368.

[4] Nordberg A (2007) Amyloid imaging in Alzheimer's disease. *Curr Opin Neurol* **20**, 398-402.

[5] Mintun MA, Larossa GN, Sheline YI, Dence CS, Lee SY, Mach RH, Klunk WE, Mathis CA, DeKosky ST, Morris JC (2006) [11C]PIB in a nondemented population: potential antecedent marker of Alzheimer disease. *Neurology* **67**, 446-452.

[6] Furumoto S, Okamura N, Iwata R, Yanai K, Arai H, Kudo Y (2007) Recent advances in the development of amyloid imaging agents. *Curr Top Med Chem* **7**, 1773-1789.

[7] Okamura N, Suemoto T, Shimadzu H, Suzuki M, Shiomitsu T, Akatsu H, Yamamoto T, Staufenbiel M, Yanai K, Arai H, Sasaki H, Kudo Y, Sawada T (2004) Styrylbenzoxazole derivatives for *in vivo* imaging of amyloid plaques in the brain. *J Neurosci* **24**, 2535-2541.

[8] Klunk WE, Engler H, Nordberg A, Wang Y, Blomqvist G, Holt DP, Bergstrom M, Savitcheva I, Huang GF, Estrada S, Ausen B, Debnath ML, Barletta J, Price JC, Sandell J, Lopresti BJ, Wall A, Koivisto P, Antoni G, Mathis CA, Langstrom B (2004) Imaging brain amyloid in Alzheimer's disease with Pittsburgh Compound-B. *Ann Neurol* **55**, 306-319.

[9] Small GW, Kepe V, Ercoli LM, Siddarth P, Bookheimer SY, Miller KJ, Lavretsky H, Burggren AC, Cole GM, Vinters HV, Thompson PM, Huang SC, Satyamurthy N, Phelps ME, Barrio JR (2006) PET of brain amyloid and tau in mild cognitive impairment. *N Engl J Med* **355**, 2652-2663.

[10] Verhoeff NP, Wilson AA, Takeshita S, Trop L, Hussey D, Singh K, Kung HF, Kung MP, Houle S (2004) *In-vivo* imaging of Alzheimer disease beta-amyloid with [11C]SB-13 PET. *Am J Geriatr Psychiatry* **12**, 584-595.

[11] Kudo Y, Okamura N, Furumoto S, Tashiro M, Furukawa K, Maruyama M, Itoh M, Iwata R, Yanai K, Arai H (2007) 2-(2-[2-Dimethylaminothiazol-5-yl]ethenyl)-6-(2-[fluoro]ethoxy)benzoxazole: a novel PET agent for *in vivo* detection of dense amyloid plaques in Alzheimer's disease patients. *J Nucl Med* **48**, 553-561.

[12] Nyberg S, Jonhagen ME, Cselenyi Z, Halldin C, Julin P, Olsson H, Freund-Levi Y, Andersson J, Varnas K, Svensson S, Farde L (2009) Detection of amyloid in Alzheimer's disease with positron emission tomography using [11C]AZD2184. *Eur J Nucl Med Mol Imaging* **36**, 1859-1863.

[13] Rowe CC, Ackerman U, Browne W, Mulligan R, Pike KL, O'Keefe G, Tochon-Danguy H, Chan G, Berlangieri SU, Jones G, Dickinson-Rowe KL, Kung HP, Zhang W, Kung MP, Skovronsky D, Dyrks T, Holl G, Krause S, Friebe M, Lehman L, Lindemann S, Dinkelborg LM, Masters CL, Villemagne VL (2008) Imaging of amyloid beta in Alzheimer's disease with 18F-BAY94-9172, a novel PET tracer: proof of mechanism. *Lancet Neurol* **7**, 129-135.

[14] Nelissen N, Van Laere K, Thurfjell L, Owenius R, Vandenbulcke M, Koole M, Bormans G, Brooks DJ, Vandenberghe R (2009) Phase 1 study of the Pittsburgh compound B derivative 18F-flutemetamol in healthy volunteers and patients with probable Alzheimer disease. *J Nucl Med* **50**, 1251-1259.

[15] Choi SR, Golding G, Zhuang Z, Zhang W, Lim N, Hefti F, Benedum TE, Kilbourn MR, Skovronsky D, Kung HF (2009) Preclinical properties of 18F-AV-45: a PET agent for Abeta plaques in the brain. *J Nucl Med* **50**, 1887-1894.

[16] Okamura N, Fodero-Tavoletti MT, Kudo Y, Rowe CC, Furumoto S, Arai H, Masters CL, Yanai K, Villemagne VL (2009) Advances in molecular imaging for the diagnosis of dementia. *Expert Opin Med Diagn* **3**, 705-716.

[17] Raymond SB, Skoch J, Hills ID, Nesterov EE, Swager TM, Bacskai BJ (2008) Smart optical probes for near-infrared fluorescence imaging of Alzheimer's disease pathology. *Eur J Nucl Med Mol Imaging* **35**, S93-S98.

[18] Hintersteiner M, Enz A, Frey P, Jaton AL, Kinzy W, Kneuer R, Neumann U, Rudin M, Staufenbiel M, Stoeckli M, Wiederhold KH, Gremlich HU (2005) *In vivo* detection of amyloid-beta deposits by near-infrared imaging using an oxazine-derivative probe. *Nat Biotechnol* **23**, 577-583.

[19] Nesterov EE, Skoch J, Hyman BT, Klunk WE, Bacskai BJ, Swager TM (2005) *In vivo* optical imaging of amyloid aggregates in brain: design of fluorescent markers. *Angew Chem Int Ed Engl* **44**, 5452-5456.

[20] Ran C, Xu X, Raymond SB, Ferrara BJ, Neal K, Bacskai BJ, Medarova Z, Moore A (2009) Design, synthesis, and testing of difluoroboron-derivatized curcumins as near-infrared probes for *in vivo* detection of amyloid-beta deposits. *J Am Chem Soc* **131**, 15257-15261.

[21] Mathis CA, Bacskai BJ, Kajdasz ST, McLellan ME, Frosch MP, Hyman BT, Holt DP, Wang Y, Huang GF, Debnath ML, Klunk WE (2002) A lipophilic thioflavin-T derivative for positron emission tomography (PET) imaging of amyloid in brain. *Bioorg Med Chem Lett* **12**, 295-298.

[22] Mathis CA, Wang Y, Holt DP, Huang GF, Debnath ML, Klunk WE (2003) Synthesis and evaluation of 11C-labeled 6-substituted 2-arylbenzothiazoles as amyloid imaging agents. *J Med Chem* **46**, 2740-2754.

# Early Detection and Rehabilitation Technologies for Dementia:

## Neuroscience and Biomedical Applications

Jinglong Wu
*Okayama University, Japan*

Medical Information Science
REFERENCE

| | |
|---|---|
| Senior Editorial Director: | Kristin Klinger |
| Director of Book Publications: | Julia Mosemann |
| Editorial Director: | Lindsay Johnston |
| Acquisitions Editor: | Erika Carter |
| Development Editor: | Myla Harty |
| Production Coordinator: | Jamie Snavely |
| Typesetters: | Mike Brehm, Jennifer Romanchak and Deanna Jo Zombro |
| Cover Design: | Nick Newcomer |

Published in the United States of America by
Medical Information Science Reference (an imprint of IGI Global)
701 E. Chocolate Avenue
Hershey PA 17033
Tel: 717-533-8845
Fax: 717-533-8661
E-mail: cust@igi-global.com
Web site: http://www.igi-global.com/reference



Library of Congress Cataloging-in-Publication Data

Early detection and rehabilitation technologies for dementia: neuroscience and biomedical applications / Jinglong Wu, editor.
p. ; cm.
Includes bibliographical references and index.
Summary: "This book provides a comprehensive collection for experts in the Neuroscience and Biomedical technology fields, outlining various concepts from cognitive neuroscience and dementia to neural technology and rehabilitation"--Provided by publisher.
ISBN 978-1-60960-559-9 (hardcover) -- ISBN 978-1-60960-560-5 (ebook) 1. Dementia--Diagnosis. 2. Neurologic examination. I. Wu, Jinglong, 1958-
[DNLM: 1. Dementia. 2. Brain--physiopathology. 3. Diagnostic Techniques, Neurological. 4. Early Diagnosis. WM 220]
RC521.E27 2011
616.8'3--dc22

2010054442

British Cataloguing in Publication Data
A Cataloguing in Publication record for this book is available from the British Library.

# Chapter 28
# Noninvasive Detection of Misfolded Proteins in the Brain Using [$^{11}$C]BF-227 PET

**Nobuyuki Okamura**
*Department of Pharmacology, Tohoku University, Japan*

**Hiroyuki Arai**
*Institute of Development, Aging and Cancer, Tohoku University, Japan*

**Shozo Furumoto**
*Department of Pharmacology & Cyclotron and Radioisotope Center, Tohoku University, Japan*

**Yukitsuka Kudo**
*Innovation of New Biomedical Engineering Center, Tohoku University, Japan*

**Manabu Tashiro**
*Cyclotron and Radioisotope Center, Tohoku University, Japan*

**Kazuhiko Yanai**
*Department of Pharmacology, Tohoku University, Japan*

**Katsutoshi Furukawa**
*Institute of Development, Aging and Cancer, Tohoku University, Japan*

## ABSTRACT

*Alzheimer's disease (AD) and many other neurodegenerative disorders belong to the family of protein misfolding diseases. These diseases are characterized by the deposition of insoluble protein aggregates containing an enriched β-sheet structure. To evaluate PET amyloid-imaging tracer [$^{11}$C]BF-227 as an agent for in vivo detection of various kinds of misfolded protein, a [$^{11}$C]BF-227 PET study was performed in patients with various protein misfolding diseases, including AD, frontotemporal dementia (FTD), dementia with Lewy bodies (DLB), sporadic Creutzfeldt-Jakob disease (sCJD) and Gerstmann-Sträussler-Scheinker disease (GSS). BF-227 binds to β-amyloid fibrils with high affinity. Most of the AD patients showed prominent retention of [$^{11}$C]BF-227 in the neocortex. In addition, neocortical retention of BF-227 was observed in the subjects with mild cognitive impairment who converted to AD during*

DOI: 10.4018/978-1-60960-559-9.ch028

*follow-up. DLB patients had elevated [$^{11}$C]BF-227 uptake in the neocortex. However, FTD and sCJD patients showed no cortical retention of [$^{11}$C]BF-227. Patients with multiple system atrophy had elevated BF-227 binding in the putamen. Finally, GSS patients had elevated BF-227 uptake in the cerebellum and other brain regions. This chapter confirms that BF-227 can selectively bind to α-synuclein and prion protein deposits using postmortem brain samples. Based on these findings, [$^{11}$C]BF-227 is not necessarily specific for β-amyloid in AD patients. However, this tracer could be used to detect various types of protein aggregates in the brain.*

## INTRODUCTION

Alzheimer's disease (AD) is the most common cause of dementia in the elderly. AD currently affects 4 million people in the United States and 15 million people globally. This disease begins insidiously with mild memory problems and progresses to the development of functional impairment in multiple cognitive domains within a few years. It is important to develop diagnostic methods that have adequate sensitivity and specificity to distinguish those who are likely to develop AD from those memory-impaired individuals who will not. The pathological hallmarks of AD are the deposition of senile plaques (SPs) and neurofibrillary tangles (NFTs) (Vickers et al., 2000). SPs and NFTs are mainly composed of β-amyloid (Aβ) protein and hyperphosphorylated tau protein, respectively. Aβ is a 4 kDa 39–43 amino acid metalloprotein product derived from the proteolytic cleavage of the amyloid precursor protein (APP) by β- and γ-secretases. The abnormal accumulation of SPs has been implicated as a central event in the etiology and the pathogenesis of AD and precedes the cognitive deterioration observed in AD (Okamura et al., 2008). Tau proteins accumulate in the neuronal cytoplasm and form NFTs with age. The initial lesions leading to NFTs occur in the transentorhinal cortex, followed by involvement of the entorhinal cortex and hippocampus, progressing to the neocortex. In vivo detection of SPs and NFTs in the brain enables the detection of AD patients in the pre-symptomatic stage. Noninvasive measurement of the amount of Aβ and tau deposits in the living brain is desirable for preventive interventions and assessment of therapeutic effects.

The density of SPs in brain tissue can be measured by molecular imaging techniques using positron emission tomography (PET) and a specific radiotracer. As Aβ deposits in the AD brain generally include the β-sheet fibrillar structure, many β-sheet binding agents have been developed as Aβ binding radiotracers for PET imaging. Currently, the most successful amyloid-binding agent is N-methyl-[$^{11}$C]2-(4'-methylaminophenyl)-6-hydroxybenzothiazol (PIB), which has been shown to possess a high affinity for Aβ fibrils. PIB-PET studies in human subjects have shown a robust difference between the retention pattern in AD patients and healthy controls, with AD cases showing significantly higher retention of PIB in the neocortical areas of the brain affected by Aβ deposition (Klunk et al., 2004). PIB retention in the neocortical areas is correlated with the Aβ plaque load (Ikonomovic et al., 2008). Benzoxazole derivatives are also promising alternatives for amyloid-imaging probes (Okamura et al., 2004; Furumoto et al., 2007). A PET study using $^{11}$C-labeled 2-(2-[2-dimethylaminothiazol-5-yl]ethenyl)-6-(2-[fluoro]ethoxy) benzoxazole (BF-227) demonstrated retention of this tracer in the cerebral cortices of AD patients but not in those of normal subjects. AD patients were clearly distinguishable from normal individuals using neocortical uptake of [$^{11}$C]BF-227 (Kudo et al., 2007). Neocortical retention of BF-227 was observed in the subjects with mild cognitive impairment (MCI). BF-227 PET showed higher specificity and sensitivity than FDG-PET and

voxel-based morphometric analysis of MRI for differentiating between AD patients and normal controls, and between MCI converters and non-converters (Waragai et al., 2009; Furukawa et al., 2010). A voxel-by-voxel analysis demonstrated a higher retention of [$^{11}$C]BF-227, mainly in the posterior association cortex of AD patients and MCI converters. This distribution pattern corresponds well with the distribution of neuritic plaque deposits in postmortem AD brains. These findings suggest that [$^{11}$C]BF-227 is a promising PET probe for in vivo detection of dense amyloid deposits in AD patients.

AD and many other neurodegenerative disorders, including frontotemporal dementia (FTD), progressive supranuclear palsy, corticobasal degeneration, Parkinson's disease (PD), dementia with Lewy bodies (DLB), multiple system atrophy, and prion disease, belong to the family of protein misfolding diseases characterized by protein self-aggregation and deposition (Table 1). The tissue deposits observed in the brain in these diseases usually contain an enriched β-sheet structure, suggesting a potential target for non-invasive imaging using β-sheet binding agents. Thus, molecular PET imaging has the potential to be extended to this wide spectrum of protein misfolding diseases (Okamura et al., 2005; Okamura et al., 2009). The purpose of this study was to evaluate the clinical utility of [$^{11}$C]BF-227 PET for the noninvasive detection of misfolded proteins in the brain.

## EXPERIMENT

### Subjects

[$^{11}$C]BF-227 PET study was performed in 12 elderly normal controls, 14 patients with Alzheimer's disease (AD) and 12 subjects with mild cognitive impairment (MCI). The [$^{11}$C]BF-227 PET study was additionally performed in patients with frontotemporal dementia (FTD), dementia with Lewy bodies (DLB), multiple system atrophy (MSA), sporadic *Creutzfeldt-Jakob disease* (sCJD) and *Gerstmann-Sträussler-Scheinker* disease (GSS). The MCI subjects were divided into two groups: MCI converters (n=6) and MCI non-converters (n=7). The MCI converters were defined as patients who eventually developed AD within a mean follow-up of 27.0±7.9 months (range 14–30 months). The MCI non-converters were defined as having a transient memory loss or remaining cognitively stable through at least a two-year follow-up (27.7±2.2 months; range 25–30 months).

*Table 1. Protein misfolding diseases and their fibrillar deposits*

| Protein | Fibrillar deposits | Diseases |
|---|---|---|
| Amyloid-β | Senile plaque<br>Cerebrovascular amyloid | Alzheimer's disease<br>Down syndrome<br>Cerebral amyloid angiopathy |
| Tau | Neurofibrillary tangle<br>Pick body<br>Tufted astrocytes<br>Astrocytic plaque | Alzheimer's disease<br>Frontotemporal lobar degeneration<br>Progressive supranuclear palsy<br>Corticobasal degeneration |
| α-synuclein | Lewy body<br>Glial cytoplasmic Inclusions | Parkinson's disease<br>Dementia with Lewy bodies<br>Multiple system atrophy |
| Prion | Prion plaque | Creutzfeldt-Jakob disease<br>Gerstmann-Sträussler-Scheinker disease |

## Method

[$^{11}$C]BF-227 was synthesized from its precursor by N-methylation in dimethyl sulfoxide using [$^{11}$C]methyl triflate, as previously described (Kudo et al., 2007). The [$^{11}$C]BF-227 PET study was performed using a SET-2400W PET scanner (Shimadzu, Kyoto, Japan). After intravenous injection of 211–366 MBq [$^{11}$C]BF-227, dynamic PET images were obtained for 60 min (23 sequential scans; 5 scans × 30 s, 5 scans × 60 s, 5 scans × 150 s, and 8 scans × 300 s) with closed eyes. The standardized uptake value (SUV) was calculated by normalizing tissue concentrations by injected dose and body weight. Regions of interest (ROIs) were placed on co-registered axial MR images. The ROI information was then copied onto the PET images, and regional SUV values were sampled. The ratio of regional SUV to cerebellar SUV (SUVR) between 40 and 60 min post administration was calculated as an index of [$^{11}$C]BF-227 retention. For the analysis of prion disease data, we calculated regional to pons SUV ratio (SUVRp). For the analysis of MSA patient data, the distribution volume of [$^{11}$C]BF-227 was calculated by Logan's graphical analysis using arterial blood sample data. The protocol of this study was approved by the Committee on Clinical Investigation at Tohoku University School of Medicine and by the Advisory Committee on Radioactive Substances at Tohoku University. Written informed consent was obtained from all patients and control subjects after a complete description of the study. The clinical study was performed in accordance with the Declaration of Helsinki.

## RESULTS

A PET study using [$^{11}$C]BF-227 demonstrated the retention of this tracer in the cerebral cortices of AD patients and MCI converters to AD but not in normal subjects or MCI non-converters (Figure 1). The average neocortical SUVR in BF-227 PET was significantly higher in the AD patients and MCI converters than in the normal subjects and MCI non-converters (Figure 2). We further examined BF-227 PET scans in patients with FTD, PD and DLB. Although imaging in FTD and PD patients showed normal distribution of BF-227 in the brain, DLB patients had moderate neocortical retention of BF-227 (Figure 1). Intriguingly, imaging from MSA patients showed BF-227 retention in the putamen, cerebral cortex and subcortical white matter. Microscopic examination indicates that BF-227 selectively binds to intracellular α-synuclein deposits, called glial cytoplasmic inclusions (GCIs), in MSA brain sections (Figure 3). Finally, significantly higher retention of BF-227 was detected in the cerebellum of GSS patients compared with that of normal controls and AD patients (Figure 4). In contrast, sCJD patients showed no obvious BF-227 retention in the cerebellum. Selective binding of BF-227 to prion protein plaques was confirmed using brain samples from autopsy-confirmed GSS cases (Figure 4).

## DISCUSSION

Our study demonstrated that [$^{11}$C]BF-227 PET is useful for the in vivo detection of Aβ and prion protein plaques in the human brain. BF-227 PET achieved high diagnostic accuracy in discriminating between MCI converters and non-converters. This result strongly suggests that [$^{11}$C]BF-227 PET would be useful to predict conversion from MCI to AD. Regarding the binding of PET imaging agents to prion proteins, a previous PET study demonstrated a moderate level of FDDNP retention and no remarkable PIB retention in the brain of familial CJD patients (Boxer et al., 2007). Another PET study also demonstrated that PIB was not specifically retained in two sCJD patients (Villemagne et al., 2009). In comparison with these previous studies, BF-227 successfully

*Figure 1. [$^{11}$C]BF-227 PET images in an elderly normal control, a patient with Alzheimer's disease (AD), a MCI non-converter, a MCI converter, a patient with frontotemporal dementia (FTD) and a patient with dementia with Lewy bodies (DLB).*

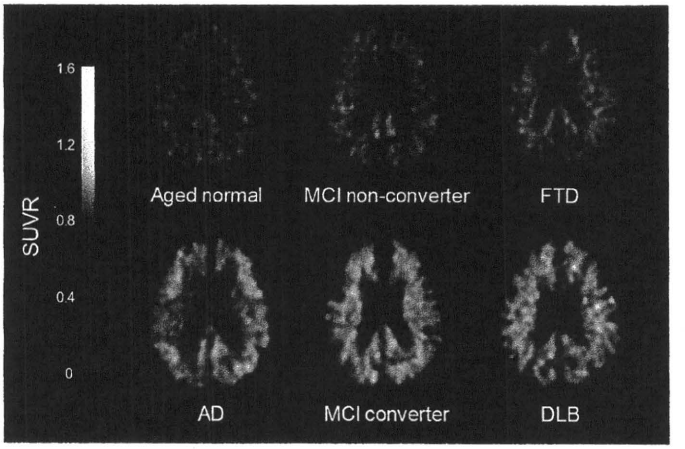


*Figure 2. Average neocortical SUVR values in elderly normal controls (AN), MCI non-converters (MCI-NC), MCI converters (MCI-C), and patients with Alzheimer's disease (AD). *p<0.05, ANOVA followed by a Bonferroni multiple comparisons test.*

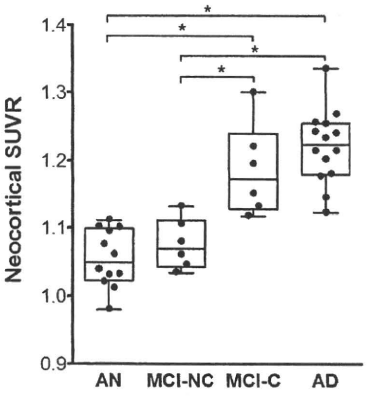


visualized prion protein plaques in the brains of GSS patients. Histopathological studies indicate a higher density of prion protein plaques in GSS patients than in familial CJD patients (Okamura et al., 2010). Therefore, the differences between our findings and those of previous studies would mainly depend upon the amount of prion protein fibrils in the brain. The difference might also be attributable to higher binding affinity of BF-227 to prion protein plaques compared to the other PET probes. Further analysis is necessary to compare the variable binding affinity of different PET probes for prion protein fibrils.

PET and microscopic studies also demonstrated that BF-227 has a potential ability to bind to and detect α-synuclein protein deposits in the brain. Previous PIB-PET studies have shown neocortical tracer accumulation in the brains of DLB patients. However, an in vitro binding study indicated that PIB failed to stain Lewy bodies in DLB brain sections. Considering the smaller size and lower density of Lewy bodies within the brains of DLB subjects relative to amyloid plaques, the contribution of Lewy bodies to the PET signals would be negligible. A recent study demonstrated that [$^{18}$F]BF-227 binds α-synuclein fibrils (Kd = 9.63 nM) with high affinity (Fodero-Tavoletti et al., 2009). Moreover, BF-227 labeled Lewy bodies and GCIs in fluorescence and immunohistochemical analyses of human brain sections, suggesting that BF-227 has higher binding affinity to α-synuclein deposits than PIB. Elevated BF-227 uptake was

*Figure 3. (A): [$^{11}$C]BF-227 PET images in a normal control subject (Control) and a patient with multiple system atrophy (MSA). (B and C): Microscopic images of BF-227 staining (B) and α-synuclein immunostaining (C) of the cerebellar white matter of a MSA case. Bar = 100 μm.*

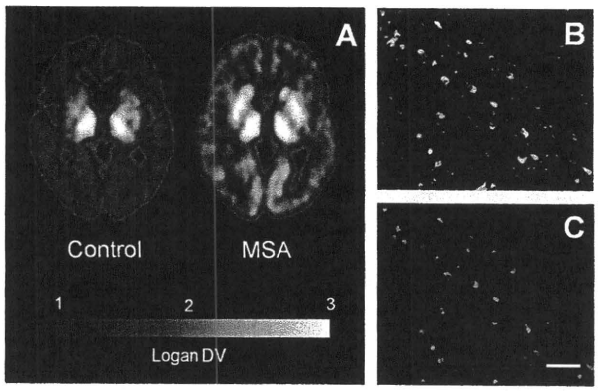


*Figure 4. (A): The regional to pons SUV ratio (SUVRp) values in the cerebella of 10 normal controls, 17 patients with Alzheimer's disease (AD), 2 patients with sporadic Creutzfeldt-Jakob disease (sCJD), and 3 patients with Gerstmann-Sträussler-Scheinker disease (GSS). (B and C): Microscopic images of BF-227 staining (B) and PrP immunostaining (C) of the cerebellar cortex of a GSS case. Bar = 25 μm.*

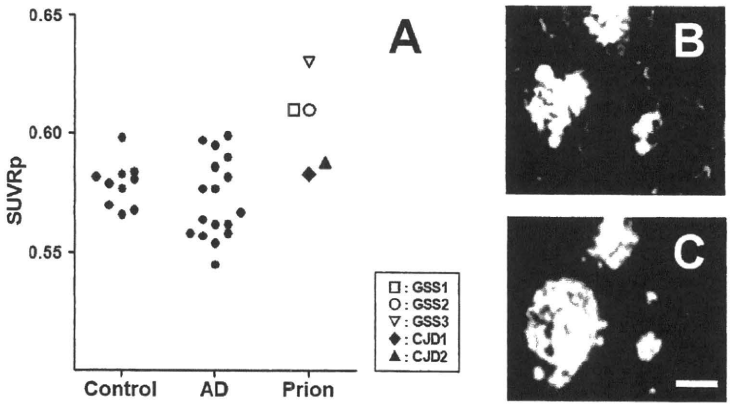


observed in the brains of MSA patients, which contain more α-synuclein deposits than those of DLB patients (Kikuchi et al., 2010). Further clinical studies of patients with α-synucleinopathy will clarify the potential of BF-227 for noninvasive detection of α-synuclein deposits in the human brain. From these findings, we conclude that BF-227 PET provides a potential method to facilitate both early diagnosis and noninvasive monitoring of protein misfolding diseases.

## ACKNOWLEDGMENT

Part of this study was supported by the Health and Labor Sciences Research Grants for Translational Research from the Ministry of Health and the